

University of Groningen

Adaptation to Unknown Leader Velocity in Vector-field UAV Formation

Baldi, Simone; Sun, Danping; Zhou, Guopeng ; Liu, Di

Published in:
IEEE Transactions on Aerospace and Electronic Systems

DOI:
[10.1109/TAES.2021.3103583](https://doi.org/10.1109/TAES.2021.3103583)

IMPORTANT NOTE: You are advised to consult the publisher's version (publisher's PDF) if you wish to cite from it. Please check the document version below.

Document Version
Publisher's PDF, also known as Version of record

Publication date:
2022

[Link to publication in University of Groningen/UMCG research database](#)

Citation for published version (APA):

Baldi, S., Sun, D., Zhou, G., & Liu, D. (2022). Adaptation to Unknown Leader Velocity in Vector-field UAV Formation. *IEEE Transactions on Aerospace and Electronic Systems*, 58(1), 473-484.
<https://doi.org/10.1109/TAES.2021.3103583>

Copyright

Other than for strictly personal use, it is not permitted to download or to forward/distribute the text or part of it without the consent of the author(s) and/or copyright holder(s), unless the work is under an open content license (like Creative Commons).


The publication may also be distributed here under the terms of Article 25fa of the Dutch Copyright Act, indicated by the "Taverne" license. More information can be found on the University of Groningen website: <https://www.rug.nl/library/open-access/self-archiving-pure/taverne-amendment>.

Take-down policy


If you believe that this document breaches copyright please contact us providing details, and we will remove access to the work immediately and investigate your claim.


Downloaded from the University of Groningen/UMCG research database (Pure): <http://www.rug.nl/research/portal>. For technical reasons the number of authors shown on this cover page is limited to 10 maximum.

Adaptation to Unknown Leader Velocity in Vector-Field UAV Formation

SIMONE BALDI , Senior Member, IEEE
Southeast University, Nanjing, China, and also Delft University of Technology, Delft, The Netherlands

DANPING SUN 
Wuhan Textile University, Wuhan, China

GUOPENG ZHOU 
Hubei University of Science and Technology, Xianning, China

DI LIU 
Southeast University, Nanjing, China, and also University of Groningen, Groningen, The Netherlands

This article presents a new adaptive method for formation control of unmanned aerial vehicles (UAVs) with limited leader information and communication. We study a formation control protocol in the framework of vector-field guidance where the leader can communicate its position and orientation but not its velocity. A practical motivation for this scenario is the so-called congestion-aware control, in which tradeoffs between the density of unmanned vehicles and communication interference caused by many communicating vehicles arise: these tradeoffs may require to reduce the communication load to avoid

Manuscript received January 21, 2021; revised April 29, 2021; released for publication July 12, 2021. Date of publication September 23, 2021; date of current version February 10, 2022.

DOI: No. 10.1109/TAES.2021.3103583

Refereeing of this contribution was handled by H.-S. Shin.

This work was supported in part by the Double Innovation Plan under Grant 4207012004, in part by the Special Funding for Overseas Talents under Grant 6207011901, in part by the Natural Science Foundation of China under Grant 62073074, and in part by the Science and Technology Plan Project of Hubei Province (second batch) under Grant 2019BEC206.

Authors' addresses: Simone Baldi is with School of Mathematics, Southeast University, Nanjing 210096, China, and also with the Delft Center for Systems and Control, Delft University of Technology, CD 2628, Delft, The Netherlands, E-mail: (s.baldi@tudelft.nl); Danping Sun is with Wuhan Textile University, Wuhan 430200, China, E-mail: (sunsundp24@163.com); Guopeng Zhou is with Hubei University of Science and Technology, Xianning 437100, China, E-mail: (zhgpeng@hbust.edu.cn); Di Liu is with School of Cyber Science and Engineering, Southeast University, Nanjing 210096, China, and also with the Bernoulli Institute for Mathematics, Computer Science and Artificial Intelligence, University of Groningen, 9712 Groningen, The Netherlands, E-mail: (di.liu@rug.nl). (*Corresponding authors: Guopeng Zhou; Di Liu.*)

0018-9251 © 2021 IEEE

interference. To compensate for the lack of knowledge of the leader velocity, each UAV makes use of a local estimation mechanism. The resulting method is an adaptive control method, whose stability can be established using Lyapunov stability. We show that the method can be extended to a distributed communication setting with a few neighboring UAVs in place of the leader. Extensive simulations with different formation shapes (Y, V, and T formation) show that the proposed adaptation mechanism effectively achieves the formation despite the unknown leader velocity. The proposed mechanism has a very similar performance to the ideal case when the leader velocity is perfectly known, and outperforms all the nonadaptive cases in which the followers have an incorrect knowledge of the leader velocity.

I. INTRODUCTION

Formation flight technology for unmanned aerial vehicles (UAVs) is a relevant but challenging topic, studied by many scholars, institutes, and companies around the world [1]–[3]. Formation flight forms the basis for cooperative operation, cooperative search and rescue, or cooperative exploration in unknown environments [4]–[6]. Different formations can have different practical use: common formations can be straight-line shape, circular shape, V-shape, and other shapes, sometimes inspired by formations of birds. For example, studies have shown that V-shapes can reduce fuel consumption and increase flight range by means of upwash airflow; straight-line shapes can be used to navigate through obstacles like narrow valleys; circular shapes can be used to attack targets cooperatively [7].

Researchers have proposed different methods for path planning of single UAVs and for formations of UAVs [8]–[10]. When considering path planning of single UAVs, wind disturbance [11], uncertain dynamic characteristics of the UAV, and sensor quality are major difficulties [12]. In this work, we address the influence of wind via the so-called vector-field path planning, which is a popular approach originally presented in [13] and [14] and now adopted in many autonomous vehicles (aerial, ground, surface, and underwater [15]–[20]). Several variants to the standard vector-field approach have been proposed in the literature. In [21], an adaptive vector-field approach is proposed to handle unknown and slowly time-varying wind. The results in [22] demonstrate that an adaptive vector-field can also counteract the presence of unmodeled course angle dynamics. In this work, we aim to study adaptation in formation control tasks, and in particular adaptation to unknown leader velocity in vector-field formations of UAVs.

Many formation control methods have been proposed and tested on semiphysical or actual UAV platforms [23]–[25]. A formation protocol for UAV swarming was proposed in [26], a formation-containment protocol was studied in [27]. The potential-field approach, which is closely related to the vector-field idea, was studied in [28]. The authors in [29] integrated formation control, trajectory tracking, and obstacle avoidance into a unified framework, via inverse optimal control. It is clear that communication is a crucial aspect for formations of UAVs. At the same time, the communication should be kept as limited as possible so as to avoid communication interference among connected vehicles [30], [31]. The issue of saving communication in

unmanned vehicles has been overlooked for a long time in the literature, but it has attracted some attention recently: for example, for connected ground vehicles it has been shown that there are tradeoffs between the density of vehicles and the interference caused by many vehicles communicating with each other: these tradeoffs require congestion-aware formation control methods [34], [35].

Unfortunately, standard protocols for formation control, that can be grouped into two families, neglect this aspect. In the first family of protocols, the leader or the follower UAVs can communicate all of their states among each other (position, velocity, orientation, linear, and angular velocity) [25], [36]–[38], which can lead to high communication overhead; in the second family of protocols, it is assumed that the leader UAV has unknown states and therefore a distributed observer is designed to estimate the unknown states [39]–[41]. Unfortunately, standard distributed observers also requires the communication of extra variables, which are the auxiliary states of the distributed observer: communication of these variables will inevitably lead to high communication overhead. In addition, not all proposed distributed observers can be applied to UAVs: for examples, the distributed observers in [42] and [43] apply to linear or fully actuated Euler-Lagrange dynamics, whereas UAV dynamics are nonlinear and under-actuated. Dynamics of mobile robots are nonlinear and under-actuated [44], [45], but the control of the course in a mobile robot is different from the control of the course in a UAV, due to the presence of a low-level autopilot [13] which is not present in a mobile robot. It should be also mentioned that distributed estimators for mobile robots use a sliding-mode approach (i.e., a sign function in the estimator) [44], [45]: from a practical point of view, the presence of a sign function requires very fast communication in order to measure at every time step if the sign of the error is positive or negative. Fast communication is in general not possible in UAVs.

Motivated by these challenges, we propose a different approach: we study a formation control protocol in which the leader can communicate only its position and orientation. Its velocity is not communicated and it is estimated locally by each UAV. The main contributions are summarized as follows:

- 1) Achieving formation of multiple UAVs even when the velocity of the leader is unknown. The dynamics under consideration are nonlinear guidance dynamics [13], which differ from the typical dynamics of mobile robots.
- 2) Designing a local estimator suitable for UAV dynamics so that when the followers cannot get the velocity information of the leader, they can estimate the information to adapt the formation. The estimator is continuous and avoids the use of a sign function which usually requires fast communication to discern if the sign of the error is positive or negative.
- 3) Designing such estimator in such a way that it does not require communication of states of the distributed estimator or any velocity. In fact, in

the aforementioned state-of-the-art distributed observers for mobile robots [44], [45], the leader still communicates its velocity with at least one follower and this velocity is shared via consensus. In our estimator, the leader does not communicate its velocity with any of the followers.

Stability is studied in the Lyapunov framework. The situation studied in this work is that every UAV can communicate with the leader: this is motivated by the practical situation in which every UAV communicates with a ground station and therefore can get the leader information [32], [33] (we are not aware of any real-life UAV formation experiment in which the ground station is completely replaced by intervehicle communication). Nevertheless, we show that the proposed method can be extended to a distributed setting with intervehicle communication in place of leader communication.

Extensive simulations with different formation shapes (Y, V, and T shapes) show that the proposed adaptation mechanisms can effectively achieve the formation despite the unknown leader velocity. The proposed mechanism has similar performance to the ideal case when the leader velocity is perfectly known, and outperforms the nonadaptive cases in which the followers have an incorrect knowledge of the leader velocity.

The rest of the article is organized as follows. The dynamics of the system (position, velocity, and angle) are introduced in Section II. The vector field-based path tracking method for a single UAV is recalled in Section III. The formation control method of multi-UAV is presented in Section IV. Section V gives the simulation result, finally, Section VI concludes this article.

II. DYNAMIC MODEL

In this and in the next sections, the dynamics and the assumptions are taken from standard literature of vector-field path planning, stemming from [13].

ASSUMPTION 1 Altitude and airspeed (V_a) are held constant by the total energy control system (TECS) of the UAV.

ASSUMPTION 2 The UAV autopilot is equipped with a heading-hold loop so that the resulting dynamics are represented by

$$\dot{\psi} = \alpha(\psi_c - \psi) \quad (1)$$

where ψ is the heading of the UAV (the angle between its airspeed velocity and the horizontal axis in the earth frame), ψ_c is the command heading from the controller, and α is a known positive constant that characterizes the speed of response of the heading-hold autopilot loop.

Fig. 1 illustrates the effect of the wind on the course dynamics. It can be noted that the presence of wind deflects the airspeed of the UAV, so that the actual velocity of the UAV is represented by the ground velocity V_g . If the wind has two components, a constant component and a

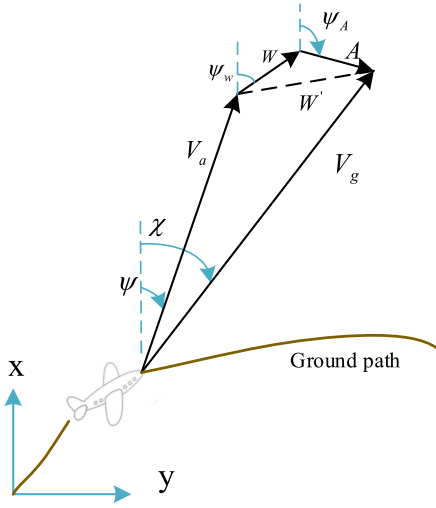


Fig. 1. Relations between airspeed, ground velocity, and wind.

possibly time-varying perturbation, both effects will sum to the airspeed.

The effect of the wind can be expressed in a mathematical way as follows:

$$\begin{aligned}\dot{x} &= V_a \cos \psi + W \cos \psi_w + A \cos \psi_A \\ \dot{y} &= V_a \sin \psi + W \sin \psi_w + A \sin \psi_A\end{aligned}\quad (2)$$

where x and y are the coordinates in the earth frame, W and A are the amplitudes of the constant wind and its time-varying part, ψ_w and ψ_A are the corresponding angles (angle between the constant or time-varying wind and the x -axis in the earth frame). In practice, the values of W and ψ_w can be obtained from ground measurements (anemometer), while $A(t)$ and $\psi_A(t)$ are actually time-varying perturbations and can be regarded as disturbances.

In view of Fig. 1, the component of the UAV velocity along the x - and y -axes be equivalently expressed as

$$\begin{aligned}\dot{x} &= V_g \cos \chi \\ \dot{y} &= V_g \sin \chi\end{aligned}\quad (3)$$

where χ is the course angle (the angle between the ground speed and the x -axis), and V_g is the UAV ground speed.

III. VECTOR-FIELD APPROACH

In the vector-field approach, ψ and χ are assumed to be measurable (the former is measured by on-board inertial measurement units, and the latter is estimated via sensor fusion with the GPS). To counteract the wind effect, the vector-field approach controls the course χ . Because the difference between ψ and χ is only the effect of the wind, they have approximately the same dynamics, that is

$$\dot{\chi} = \alpha(\chi_c - \chi) \quad (4)$$

where χ_c is the command course to be defined by the vector field. The vector-field idea amounts to constructing a vector field of desired course around the path to be tracked: the vectors in the field provide heading commands to the autopilot. To guide the UAV to the desired path, the vectors

are directed toward the path and eventually become tangent to the path itself. The vector-field method traditionally considers two types of path, straight line and orbit path, which are recalled hereafter (more complex paths can be constructed as a combination of straight lines and orbits).

A. Straight-Line Path Tracking

Let $y = ax + b$ represent the line equation of the desired path, where (x, y) are the coordinates of the UAV in the ground reference frame. Then, a path tracking error can be defined as

$$e_{py} = y - (ax + b) \quad (5)$$

with vector field described by

$$\chi_d = i\chi^\infty \frac{2}{\pi} \tan^{-1}(ke_{py}) + \tan^{-1}(a) \quad (6)$$

where k is a positive constant that influences the rate of the transition from χ^∞ to $\tan^{-1}(a)$. In (6), i defines the direction of UAV movement (when $i = 1$, the UAV goes to the negative direction of x axis, when $i = -1$, the UAV goes to the positive direction of x axis).

The meaning of χ_d in (6) is that when e_{py} is large, the UAV is directed towards the line with course angle $\chi^\infty \in (0, \frac{\pi}{2}]$; when e_{py} becomes smaller and smaller, the desired course tends to the same direction as the line.

The design of the input χ_c in (4) should be done in such a way to drive the UAV toward the path ($e_{py} \rightarrow 0$ and $\chi \rightarrow \chi_d$). Such a design is based on the choice of an appropriate Lyapunov function, which can be found in [13] and is not repeated here. The final design is

$$\begin{aligned}\chi_c &= \chi + \frac{i}{\alpha} \chi^\infty \frac{2}{\pi} \frac{k}{1 + (ke)^2} V_g (\sin \chi - \alpha \cos \chi) \\ &\quad - \frac{\kappa}{\alpha} \text{sat} \left(\frac{\tilde{\chi}}{\epsilon} \right)\end{aligned}\quad (7)$$

where sat is the saturation function

$$\text{sat}(x) = \begin{cases} x, & \text{if } |x| < 1 \\ \text{sign}(x), & \text{otherwise} \end{cases} \quad (8)$$

and $\tilde{\chi} = \chi - \chi_d$, and $\kappa > 0$, $\epsilon > 0$ are the parameters that control the transition region around the desired line.

B. Orbit Path Tracking

The strategy for orbit path following is similar to the straight line following, in the sense that the vector field is built around the desired orbit. For convenience, the position of the UAV is represented by polar coordinates, and the origin is set to the circular orbit center (c_x, c_y) . The relationship between circular coordinates and Cartesian coordinates is

$$\begin{aligned}x &= c_x + d \cos \gamma \\ y &= c_y + d \sin \gamma\end{aligned}\quad (9)$$

where the distance from the orbit center to the UAV is denoted with d , and the angular position of the UAV is denoted by γ . Let the radius of the orbit be r .

Substituting (9) into (3), the dynamics of the UAV in polar coordinates are

$$\begin{aligned}\dot{d} &= V_g \cos(\chi - \gamma) \\ \dot{\gamma} &= \frac{V_g}{d} \sin(\chi - \gamma).\end{aligned}\quad (10)$$

Similar to the straight line case, one should define a path tracking error which is simply $\tilde{d} = d - r$, and the vector field is described by

$$\chi_d = \gamma + j \left[\frac{\pi}{2} \tan^{-1}(k\tilde{d}) \right] \quad (11)$$

where k is a positive constant that influences the rate of the transition from $\gamma - \pi$ to $\gamma - \frac{\pi}{2}$. In (11), j defines the direction of UAV movement (when $j = 1$, the UAV goes counterclockwise, when $j = -1$, the UAV goes clockwise). The meaning of χ_d in (11) is that the vector field will point toward the orbit when \tilde{d} is large, while it will become more and more tangent to the orbit as \tilde{d} becomes smaller and smaller.

Similarly to (7), the design of the command course χ_c is based on the choice of an appropriate Lyapunov function which can be found in [13]. The final result of the design is

$$\chi_c = \chi + \frac{V_g}{d\alpha} \sin(\chi - \gamma) + j \frac{\beta}{\alpha} V_g \cos(\chi - \gamma) - \frac{\kappa}{\alpha} \text{sat}\left(\frac{\tilde{\chi}}{\epsilon}\right) \quad (12)$$

where $\beta = k/(1 + (k\tilde{d})^2)$.

REMARK 1 Even when the leader flies at a constant airspeed, the follower UAVs must be able to change their velocity in order to establish the formation. Therefore, in the following section we will present a method for the follower UAVs that, in addition to controlling the course, controls the velocity.

IV. UAV FORMATION PATH TRACKING

Several communication architectures can be found in the literature about formations of UAVs, mostly centralized and some distributed [46]–[48]. In this work, we consider a so-called leader-to-all communication topology in which the leader can communicate with all followers. Such a scenario is reasonable in UAV applications, since the leader UAV typically communicates with a ground station, and the ground station in return can send commands to the followers [32], [33].

The leader UAV adopts the vector-field path tracking algorithm specified in Section III. This section is devoted to defining the velocity and course commands for the follower UAVs. We proceed with the presentation along three steps: in the first step (Section IV-A), we define the relative coordinate frame between the leader and a follower UAV, where such a frame is useful to define the formation errors; in the second step (Section IV-B), we propose ideal velocity/course commands under the assumption that the follower UAVs have knowledge of the leader ground velocity V_g (e.g., thanks to communication); in the third step (Section IV-C), the knowledge of the leader ground velocity V_g is not available, and therefore the follower UAVs must

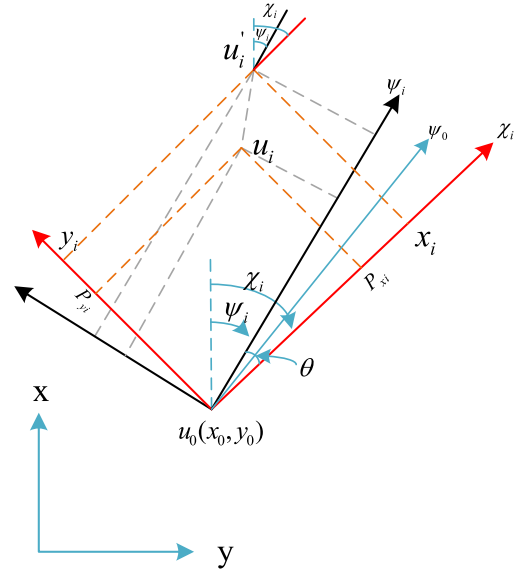


Fig. 2. Coordinate frame for leader and follower relative position. The formation can be defined with respect to the course angle χ_i , or with respect to the heading angle ψ_i . In this work, the latter is used, because it allows to control directly the follower airspeed V_{ai} .

define their velocity/course commands in combination with a local estimator. Finally, in Section IV-D, we discuss a distributed communication setting in which the leader-to-all communication is replaced by communication with a few neighboring UAVs.

A. Relative Frame Between Leader and Follower UAV

Fig. 2 describes the relative coordinate frame between a leader and a follower UAV. Take the leader UAV u_0 (with coordinates (x_0, y_0) in the global frame) as the reference zero, where the reference frame is rotated by the follower heading angle ψ_i . Then, the desired position u'_i of the follower UAV to form a shape with respect to the leader UAV is (p_{xi}, p_{yi}) , while the actual position u'_i of the follower UAV is (x_i, y_i) .

With such a configuration, the horizontal and vertical coordinates error of the relative position between each follower UAV i and the leader UAV can be denoted as $x_{ei}(t), y_{ei}(t)$, the heading angle error ψ_{ei} , which can be calculated as

$$\begin{aligned}x_{ei} &= (p_{xi} + x_0(t) - x_i(t)) \cos \psi_i(t) \\ &\quad + (p_{yi} + y_0(t) - y_i(t)) \sin \psi_i(t)\end{aligned}\quad (13)$$

$$\begin{aligned}y_{ei} &= -(p_{xi} + x_0(t) - x_i(t)) \sin \psi_i(t) \\ &\quad + (p_{yi} + y_0(t) - y_i(t)) \cos \psi_i(t)\end{aligned}\quad (14)$$

$$\psi_{ei}(t) = \psi_0(t) - \psi_i(t). \quad (15)$$

When these errors are zero, the formation, which is defined by the various (p_{xi}, p_{yi}) for each follower, is achieved. In the following we will provide the stability proof for the convergence of these errors. Two situations are discussed. In the first, the followers use the knowledge of the airspeed of the leader (e.g., obtained via communication) to reach

the formation. In the second, such knowledge is not available and each follower can automatically adjust its control according to its own situation via a local estimator.

REMARK 2 In the following, it is convenient to distinguish between two quantities: V_a and V_{a0} : the former is the actual airspeed of the leader UAV; the latter indicates what the followers think the airspeed of the leader UAV is. If the information of the follower is correct, then $V_a = V_{a0}$. If the information is incorrect (e.g. due to interference or other errors), then $V_a \neq V_{a0}$.

B. Nonadaptive VF

As standard in the vector-field literature [13], the stability analysis is performed under the assumption that V_{a0} and ψ_0 (the heading of the leader) are constant. In the case the quantities are (slowly) time-varying, i.e., their time derivative is bounded by a constant as per effect of a bounded wind disturbance or a curved path, it is natural to expect that the tracking error will not converge exactly to zero, but might be in a neighborhood of zero.

The airspeed of a follower i is denoted by V_{ai} and is a control input. Then, along similar lines as Section II we can define the dynamics for follower i as

$$\begin{aligned}\dot{x}_i(t) &= V_{ai} \cos \psi_i + W \cos \psi_w + A \cos \psi_A \\ \dot{y}_i(t) &= V_{ai} \sin \psi_i + W \sin \psi_w + A \sin \psi_A.\end{aligned}\quad (16)$$

Note that all UAVs are affected by the same wind. In addition, in line with (1), we can consider the following dynamics for the heading ψ_i :

$$\dot{\psi}_i = \alpha(\psi_{ci} - \psi_i) \quad (17)$$

where ψ_{ci} is the heading command to be designed.

If the information of the follower is correct ($V_a = V_{a0}$), the following theorem holds.

THEOREM 1 Consider the following velocity and heading controller:

$$V_{ai} = c_1 x_{ei} + V_{a0} \cos \psi_{ei} \quad (18)$$

$$\psi_{ci} = -\psi_0 + \psi_i + \psi_{c0} + \frac{c_2 \sin \psi_{ei}}{\alpha} + \frac{c_3 V_{a0} y_{ei}}{\alpha} \quad (19)$$

where c_1, c_2, c_3 are positive design scalars, and ψ_{c0} is the control heading angle of the leader UAV. Then, the errors $x_{ei}, y_{ei}, \psi_{ei}$ converge to zero as time goes to infinity.

PROOF To prove stability of (18) and (19), it is convenient to substitute them into (16), so as to obtain the dynamics

$$\begin{aligned}\dot{x}_0 - \dot{x}_i &= V_{a0} \cos \psi_0 - (c_1 x_{ei} + V_{a0} \cos \psi_{ei}) \cos \psi_i \\ \dot{y}_0 - \dot{y}_i &= V_{a0} \sin \psi_0 - (c_1 x_{ei} + V_{a0} \cos \psi_{ei}) \sin \psi_i.\end{aligned}\quad (20)$$

Also, substituting (19) into (15) gives the dynamics

$$\dot{\psi}_{ei} = -c_2 \sin \psi_{ei} - c_3 V_{a0} y_{ei}. \quad (21)$$

Consider the following Lyapunov function:

$$V = \sum_{i=1}^N V_i \quad (22)$$

with

$$V_i = \frac{1}{2} x_{ei}^2(t) + \frac{c_3}{2} y_{ei}^2(t) + (1 - \cos \psi_{ei}(t)) \quad (23)$$

$$V = \frac{1}{2} x_e^T(t) x_e(t) + \frac{c_3}{2} y_e^T(t) y_e(t) + 1_N^T (1_N - \cos \psi_e(t)) \quad (24)$$

where N is the number of follower UAVs

$$x_e(t) = [x_{e1}(t) \dots x_{eN}(t)]^T, \quad y_e(t) = [y_{e1}(t) \dots y_{eN}(t)]^T \\ 1_N = [1 \ 1 \dots 1]^T, \cos \psi_e(t) = [\cos \psi_{e1}(t) \dots \cos \psi_{eN}(t)]^T.$$

It can be noticed that the Lyapunov function is positive definite, zero at the origin, and quadratic in x_{ei}, y_{ei} .

Then, we take the derivative of the Lyapunov function

$$\begin{aligned}\dot{V} &= \sum_{i=1}^N \dot{V}_i \\ \dot{V}_i &= x_{ei} \dot{x}_{ei} + c_3 y_{ei} \dot{y}_{ei} + \dot{\psi}_{ei} \sin \psi_{ei} = -c_1 x_{ei}^2 \\ &\quad - c_2 \sin \psi_{ei}^2 \leq 0\end{aligned}$$

which is negative semidefinite, which implies that the origin $(x_{ei}, y_{ei}, \psi_{ei}) = (0, 0, 0)$ is stable. Then, using the LaSalle's lemma, we obtain that the origin is not only stable, but also asymptotically stable. This concludes the proof.

C. Proposed Adaptive VF

In this section, V_{a0} is assumed to be unknown; therefore, we define \hat{V}_{a0i} to be the estimate of V_{a0} as calculated by follower i ; each follower UAV has its own local estimator. As before, the airspeed of a follower i is denoted with V_{ai} and is a control input.

The following theorem holds.

THEOREM 2 Consider the following velocity and heading controller:

$$V_{ai} = c_1 x_{ei} + \hat{V}_{a0i} \cos \psi_{ei} \quad (25)$$

$$\psi_{ci} = -\psi_0 + \psi_i + \psi_{c0} + \frac{c_2 \sin \psi_{ei}}{\alpha} + \frac{c_3 \hat{V}_{a0i} y_{ei}}{\alpha} \quad (26)$$

and the following estimator:

$$\dot{\hat{V}}_{a0i} = c_4 (x_{ei} \cos \psi_{ei} + c_3 y_{ei} \sin \psi_{ei}) \quad (27)$$

where c_1, c_2, c_3, c_4 are positive design scalars and ψ_{c0} is the control heading angle of the leader UAV. Then, the errors $x_{ei}, y_{ei}, \psi_{ei}$ converge to zero as time goes to infinity.

PROOF Motivated by proof 1, the Lyapunov function can be chosen as

$$\begin{aligned}\bar{V} &= \frac{1}{2} x_e^T(t) x_e(t) + \frac{c_3}{2} y_e^T(t) y_e(t) + 1_N^T (1_N - \cos \psi_e(t)) \\ &\quad + \frac{1}{2c_4} \sum_{i=1}^N (\hat{V}_{a0i} - V_{a0})^T (\hat{V}_{a0i} - V_{a0}).\end{aligned}\quad (28)$$

Define $\tilde{V}_{a0i} = \hat{V}_{a0i} - V_{a0}$. It can be noticed that the Lyapunov function is positive definite and zero at the origin. As before,

let

$$V_i = \frac{1}{2}x_{ei}^2(t) + \frac{c_3}{2}y_{ei}^2(t) + (1 - \cos \psi_{ei}(t)). \quad (29)$$

Then, the time derivative can be derived as

$$\begin{aligned} \dot{V}_i &= x_{ei}\dot{x}_{ei} + c_3y_{ei}\dot{y}_{ei} + \dot{\psi}_{ei} \sin \psi_{ei} = -c_1x_{ei}^2 \\ &\quad - c_2 \sin \psi_{ei}^2 - \tilde{V}_{a0i}x_{ei} \cos \psi_{ei} - c_3\tilde{V}_{a0i}y_{ei} \sin \psi_{ei} \end{aligned} \quad (30)$$

and

$$\begin{aligned} \dot{V}_i &= \dot{V}_i + \tilde{V}_{a0i}\dot{\tilde{V}}_{a0i} = -c_1x_{ei}^2 - c_2 \sin^2 \psi_{ei} \\ &\quad - (x_{ei} \cos \psi_{ei} + c_3y_{ei} \sin \psi_{ei} - \dot{\tilde{V}}_{a0i})\tilde{V}_{a0i}. \end{aligned} \quad (31)$$

Then, thanks to the estimation law

$$\dot{V}_i = -c_1x_{ei}^2 - c_2 \sin^2 \psi_{ei} \leq 0$$

which is negative semidefinite. It is implied that the origin $(x_{ei}, y_{ei}, \psi_{ei}, \tilde{V}_{a0i}) = (0, 0, 0, 0)$ is stable. Then, using the Barbalat's lemma, we obtain that $x_{ei}, y_{ei}, \psi_{ei}$ all converge to zero as time goes to infinity. This concludes the proof.

REMARK 3 As compared to Theorem 1, the main advantage of Theorem 2 is to replace V_{a0} with the local estimate \hat{V}_{a0i} , updated by the local estimator. Therefore, the adaptive approach can compensate of lack of knowledge of V_{a0} . Major differences with respect to estimation mechanisms proposed in the literature, e.g., distributed estimators for mobile robots are the following:

- 1) The control of a course in mobile robots is different from the control of the course in UAVs, due to the presence of a low-level autopilot which is not present in mobile robots.
- 2) Distributed estimators for mobile robots use a sliding-mode approach, with a sign function in the estimator. The proposed estimator avoids this approach because, in practice, the presence of a sign function requires fast communication (not possible in UAVs) to measure at every time step if the sign of the error is positive or negative.
- 3) In distributed estimators for mobile robots, the leader still communicates its velocity with at least one follower (and this velocity is shared via consensus), whereas in our estimator the leader does not communicate its velocity with any of the followers.

D. Distributed Adaptation

The previous section has assumed a centralized setting in which every follower can communicate with the leader. Works such as [32] and [33] discuss that such a centralized setting is the most common approach due to the need for a ground station collecting the telemetry from the formation. Nevertheless, the proposed adaptation mechanism can be rearranged for a distributed setting in which UAV i communicates with one (or more) neighbors, e.g., as indicated in Fig. 3. In the following, let us index for simplicity one of such neighbors as \bar{i} .

In this setting, let $\bar{x}_{ei}, \bar{y}_{ei}, \bar{\psi}_{ei}$ represent the formation errors with such a neighbor (where the desired gap is also

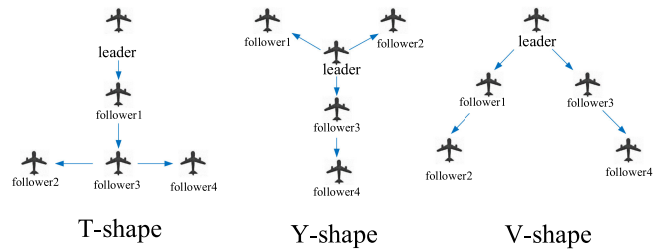


Fig. 3. Schemes of the formations and possible distributed communication topologies.

defined with respect to this neighbor). Then, let $\bar{\psi}_{\bar{i}}, \bar{\psi}_{c\bar{i}}$ be quantities from such neighbor, and let $\hat{V}_{a\bar{i}}$ represent the estimate of the velocity $V_{a\bar{i}}$ of neighbor \bar{i} , as calculated by UAV i .

Then, using similar distributed adaptive tools explored by some of the authors for linear dynamics [49], it suffices to consider the following velocity and heading controller:

$$V_{ai} = c_1\bar{x}_{ei} + \hat{V}_{a\bar{i}} \cos \bar{\psi}_{ei} \quad (32)$$

$$\psi_{ci} = -\bar{\psi}_{\bar{i}} + \psi_{ei} + \bar{\psi}_{c\bar{i}} + \frac{c_2 \sin \bar{\psi}_{ei}}{\alpha} + \frac{c_3 \hat{V}_{a\bar{i}} \bar{y}_{ei}}{\alpha} \quad (33)$$

and the following estimator:

$$\dot{\hat{V}}_{a\bar{i}} = c_4(\bar{x}_{ei} \cos \bar{\psi}_{ei} + c_3\bar{y}_{ei} \sin \bar{\psi}_{ei}) \quad (34)$$

to provide a similar stability result as Theorem 2, with distributed (instead of centralized) communication. The difference between (25)–(27) and (32)–(34) is replacing $x_{ei}, y_{ei}, \psi_{ei}$ (formation error with the leader) with $\bar{x}_{ei}, \bar{y}_{ei}, \bar{\psi}_{ei}$ (formation error with the neighbor), and replacing $\psi_{c0} - \psi_0$ (signal from leader) with $\bar{\psi}_{c\bar{i}} - \bar{\psi}_{\bar{i}}$ (signal from neighbor). A similar modification holds also for nonadaptive version (18), (19), where V_{a0i} (leader airspeed) should be replaced with $V_{a\bar{i}}$ (neighbor airspeed). To validate the feasibility of this approach, some simulations in the next section are done in such a distributed scenario.

REMARK 4 Because the method used to solve the problem relies on adaptive control theory, issues of noise and unmodeled dynamics can be solved using tools from robust adaptive control, c.f. the book [50]. The tools, not shown here due to lack of space, amount to modifying the adaptive laws by including terms such as leakage term, dead zones, or projection. These modifications provide robustness to non-parametric perturbations such as disturbances, unmodeled dynamics, and time delays. In the book [51], it is further explained that similar modifications in the adaptive laws are also useful to address time-varying parameters.

V. NUMERICAL VALIDATION

We consider different formations of five UAVs (one leader and four followers) which must achieve different shapes. Three shapes are discussed: the inverted T formation, the Y formation, and the inverted V formation, represented in Fig. 3. For simplicity, we omit the term ‘inverted’ and simply refer to the formations as T, Y, and V formation. The desired positions to achieve the formation

TABLE I
Formation Gaps Are Expressed With Respect to the Leader

| Followers | UAV #1 | UAV #2 | UAV #3 | UAV #4 |
|---------------------|---------|-----------|---------|----------|
| Line Gap(x, y) | | | | |
| T shape | (0,-7) | (-7,-14) | (0,-14) | (7,-14) |
| Y shape | (-7,7) | (7,7) | (0,-7) | (0,-14) |
| V shape | (-7,-7) | (-14,-14) | (7,-7) | (14,-14) |
| Orbit Gap(x, y) | | | | |
| T shape | (0,-4) | (-4,-8) | (0,-8) | (4,-8) |
| Y shape | (-4,4) | (4,4) | (0,-4) | (0,-8) |
| V shape | (-4,-4) | (-8,-8) | (4,-4) | (8,-8) |
| Gains | c_1 | c_2 | c_3 | c_4 |
| $\alpha = 0.6$ | 0.8 | 100 | 1 | 0.02 |

TABLE II
Straight Line Path: RMS Formation Errors for Correct ($V_{a0} = 12$) and Incorrect ($V_{a0} = 7$, $V_{a0} = 17$) Leader Speed. The Percentages Refer to the Increased Error of the Nonadaptive VF as Compared to the Corresponding Adaptive VF (Only in One Case the Nonadaptive VF Is 0.2% Better Than Adaptive)

| $V_{a0} = 12$ | Shape | #1 | #2 | #3 | #4 | total (% improv.) |
|-----------------------------------|-------|-------|-------|--------|-------|-------------------|
| non-adaptive VF: $V_{a0} = 12$ | T | 3.081 | 6.089 | 4.826 | 6.040 | 20.036 (+0.1%) |
| | Y | 4.538 | 4.588 | 3.168 | 5.094 | 17.387 (+0.4%) |
| | V | 4.818 | 4.504 | 8.053 | 4.933 | 22.308 (-0.2%) |
| adaptive VF: $V_{a0} = 12$ | T | 3.118 | 5.997 | 4.842 | 6.066 | 20.022 |
| | Y | 4.486 | 4.502 | 3.239 | 5.099 | 17.326 |
| | V | 4.797 | 4.616 | 8.082 | 4.847 | 22.343 |
| non-adaptive VF: $V_{a0} = 17$ | T | 5.791 | 7.626 | 7.006 | 7.218 | 27.640 (+13.8%) |
| | Y | 6.007 | 5.499 | 5.909 | 7.651 | 25.065 (+15.1%) |
| | V | 7.190 | 6.049 | 12.574 | 6.312 | 32.125 (+11.7%) |
| adaptive VF: $V_{a0} = 17$ | T | 4.366 | 6.884 | 5.831 | 6.736 | 23.818 |
| | Y | 5.295 | 4.855 | 4.452 | 6.669 | 21.270 |
| | V | 6.057 | 4.979 | 11.669 | 5.664 | 28.369 |
| non-adaptive VF: $V_{a0} = 7$ | T | 6.781 | 6.862 | 6.963 | 8.155 | 28.761 (+9.0%) |
| | Y | 7.968 | 8.627 | 7.000 | 7.244 | 30.838 (+14.7%) |
| | V | 7.167 | 7.974 | 9.134 | 9.185 | 33.460 (+7.7%) |
| adaptive VF: $V_{a0} = 7$ | T | 5.790 | 6.120 | 6.474 | 7.793 | 26.176 |
| | Y | 6.237 | 6.875 | 6.185 | 7.003 | 26.299 |
| | V | 6.303 | 7.048 | 8.831 | 8.689 | 30.870 |

are shown in Table I. Let us clarify that all the gains c_1 , c_2 , c_3 , c_4 are kept the same for all simulations.

To address realistic problems such as unmodeled dynamics, sensor noise, etc., the experiments make use of a software-in-the-loop UAV model developed in the past by some of the authors [22], [52]. This UAV model includes the low-level autopilot of a UAV (ArduPilot) and can capture unmodeled low-level dynamics and sensor noise. These low level controllers (e.g., roll/pitch/yaw controllers) essentially are unmodeled dynamics, since they are present in any real UAV but that do not appear in the guidance dynamics. The noise in the simulator also includes the quantization noise due to discrete-time implementation of the control. To this purpose, it is worth remarking that the communication in the simulator occurs at 10 Hz, which is very representative of real communication among UAVs or among UAVs and ground station. We perform simulations in a windy scenario

TABLE III
Orbit Path: RMS Formation Errors for Correct ($V_{a0} = 12$) and Incorrect ($V_{a0} = 7$, $V_{a0} = 17$) Leader Speed. The Percentages Refer to the Increased Error of the Nonadaptive VF as Compared to the Corresponding Adaptive VF

| $V_{a0} = 12$ | Shape | #1 | #2 | #3 | #4 | total (% improv.) |
|-----------------------------------|-------|--------|-------|--------|--------|-------------------|
| non-adaptive VF: $V_{a0} = 12$ | T | 3.291 | 6.404 | 5.077 | 6.522 | 21.295 (+1.3%) |
| | Y | 7.063 | 6.734 | 3.707 | 6.191 | 23.695 (+4.3%) |
| | V | 5.782 | 5.816 | 9.910 | 8.545 | 30.052 (+8.1%) |
| adaptive VF: $V_{a0} = 12$ | T | 3.291 | 6.414 | 5.066 | 6.239 | 21.011 |
| | Y | 5.987 | 6.802 | 3.727 | 6.159 | 22.675 |
| | V | 5.215 | 5.363 | 9.181 | 7.868 | 27.627 |
| non-adaptive VF: $V_{a0} = 17$ | T | 5.204 | 9.222 | 5.795 | 9.743 | 29.964 (+22.2%) |
| | Y | 5.009 | 7.001 | 5.823 | 7.000 | 24.833 (+7.9%) |
| | V | 4.116 | 7.334 | 9.324 | 17.604 | 38.376 (+23.0%) |
| adaptive VF: $V_{a0} = 17$ | T | 3.908 | 6.514 | 5.566 | 7.325 | 23.312 |
| | Y | 5.041 | 6.672 | 4.117 | 7.037 | 22.867 |
| | V | 4.083 | 6.372 | 9.228 | 9.852 | 29.534 |
| non-adaptive VF: $V_{a0} = 7$ | T | 7.683 | 9.082 | 7.900 | 8.092 | 32.757 (+7.0%) |
| | Y | 11.851 | 9.286 | 7.886 | 8.779 | 37.802 (+13.5%) |
| | V | 10.670 | 7.638 | 13.260 | 10.034 | 41.603 (+7.2%) |
| adaptive VF: $V_{a0} = 7$ | T | 6.423 | 8.451 | 7.529 | 8.053 | 30.456 |
| | Y | 8.729 | 8.331 | 6.985 | 8.652 | 32.697 |
| | V | 8.464 | 7.536 | 11.396 | 11.194 | 38.590 |

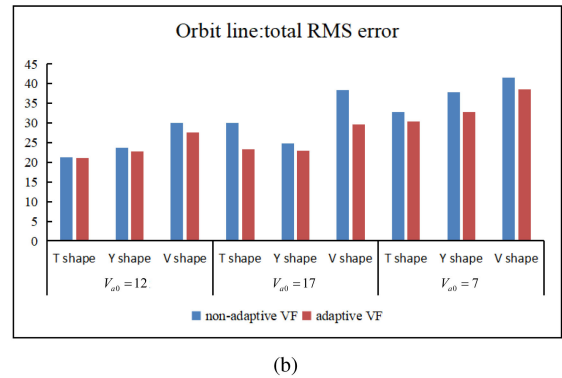
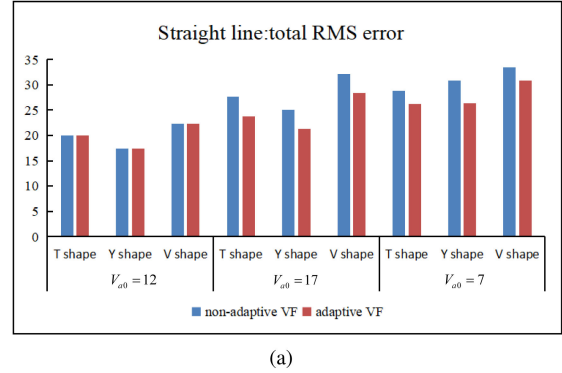


Fig. 4. Each bar of the histogram show the sum rms errors for the four follower UAVs, using communication with the leading UAV indicated in Fig. 3). The sums are given for different leader speeds and shapes. The blue bar is the nonadaptive VF, the red bar is the adaptive VF. (a) Straight line path. (b) Orbit line path.

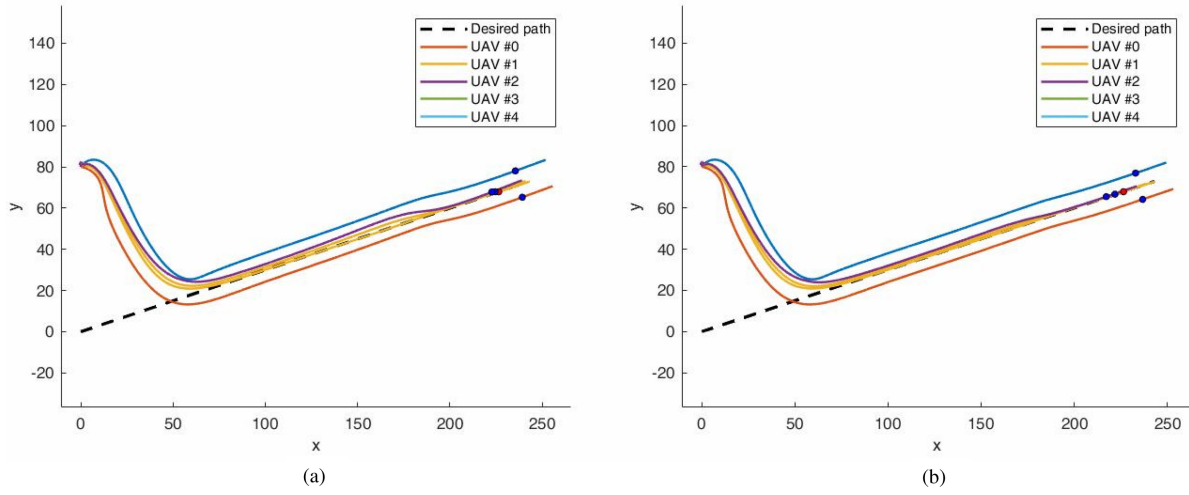


Fig. 5. Line Y formation with $V_a = 12$, $V_{a0} = 17$. The UAVs are depicted as dots at time 37 s. The leader is indicated with a red dot. In the nonadaptive case, the followers think the leader is faster than it actually is and cannot keep a good Y shape. (a) Nonadaptive VF. (b) Adaptive VF.

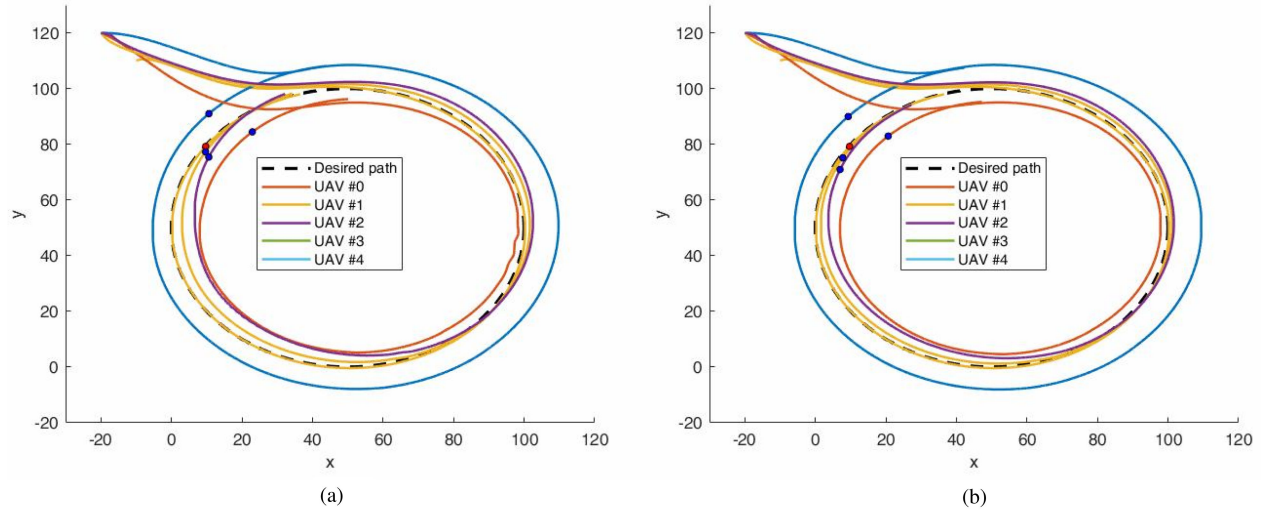


Fig. 6. Orbit Y formation with $V_a = 12$, $V_{a0} = 17$. The UAVs are depicted as dots at time 37 s. The leader is indicated with a red dot. In the nonadaptive case, the followers think the leader is faster than it actually is and cannot keep a good Y shape. (a) Nonadaptive VF. (b) Adaptive VF.

where a constant wind is perturbed by a sinusoidal wind. The wind parameters are: constant wind amplitude $W = 6\text{m/s}$; constant wind angle $\psi_w = 230^\circ$; time-varying wind amplitude $A(t) = 3 \cos(0.1t)\text{m/s}$; time-varying wind angle: $\psi_A(t) = \pi \sin(0.1t)^\circ$.

We have 3 different scenarios with T, Y, V shapes, which are tested for both the straight line and the orbit case.

- 1) VF with $V_a = V_{a0} = 12$: In this scenario (line and orbit), the leader has velocity $V_a = 12$. The followers correctly use $V_{a0} = 12$ in their control law (18), (19) all the time (nonadaptive VF) or use (25), (26) with $\hat{V}_{a0i} = 12$ as initial condition to their local estimator (27) (adaptive VF).
- 2) VF with $V_a = 12$, $V_{a0} = 17$: In this scenario (line and orbit), the leader has velocity $V_a = 12$. The followers do not have the exact knowledge and incorrectly use

$V_{a0} = 17$ in their control law (18), (19) all the time (nonadaptive VF) or use (25), (26) with $\hat{V}_{a0i} = 17$ as initial condition to their local estimator (27) (adaptive VF).

- 3) VF with $V_a = 12$, $V_{a0} = 7$: In this scenario (line and orbit), the leader has velocity $V_a = 12$. The followers do not have the exact knowledge and incorrectly use $V_{a0} = 7$ in their control law (18), (19) all the time (nonadaptive VF) or use (25), (26) with $\hat{V}_{a0i} = 7$ as initial condition to their local estimator (27) (adaptive VF).

The first scenario has the purpose of checking how close the adaptation mechanism is to the perfect knowledge case of the leader velocity. The last two scenarios have the purpose of checking if the local estimator can compensate for the incorrect knowledge of the leader velocity.

For the straight line path tracking, the target path is $y = 0.3x$. For all three shapes, the initial positions of the follower UAVs are (0,80) and the initial course angles are $0, \pi/6, \pi/3$ and $\pi/4$. For the orbit line path tracking, the target path is $(x - 50)^2 + (y - 50)^2 = 100$. For all three shapes, the initial positions of the follower UAVs are $(-20|120)$ and the initial course angles are again $0, \pi/6, \pi/3$ and $\pi/4$.

A. Discussion of Table Results

Tables II and III report the root mean square (rms) formation errors (i.e., the error with respect to the desired formation point). The rms errors are calculated for each follower UAV and then eventually summed as “total.” For better judging the performance of the adaptive mechanism as compared to the nonadaptive one, the percentage difference is calculated as

$$\frac{\text{total (non-adaptive)} - \text{total (adaptive)}}{\text{total (non-adaptive)}} \%. \quad (35)$$

When the percentage is negative, it means that the total rms error of the adaptive control is larger than the total rms error of the nonadaptive control; vice versa, a positive percentage indicates the improvement of the adaptive control over the nonadaptive one. The positive percentages are reported in bold in Tables II and III, and it can be seen that most of the time, the adaptive method improves over the nonadaptive one. The following comments hold in detail.

- 1) Only with line path and correct knowledge of leader velocity the nonadaptive control is comparable with the adaptive one (see Table II). On the other hand, for the orbit path, even with correct knowledge of leader velocity the estimator can actually lead to improved performance in the range 1.3–8.1% (see Table III).
- 2) When the followers think that the leader is faster than it actually is (17 m/s instead of 12 m/s), only the adaptive strategy can “fix” this mistake, while the nonadaptive strategy keeps the same wrong information. The adaptive mechanism leads to improvements in the range 11.7–15.1% for the line (see Table II), and in the range 7.9–23% for the orbit (see Table III).
- 3) When the followers think that the leader is slower than it actually is (7 m/s instead of 12 m/s), only the adaptive strategy can “fix” this mistake. The adaptive mechanism leads to improvements in the range 7.7–14.7% for the line (see Table II), and in the range 7–13.5% for the orbit (see Table III). The orbit path is more challenging than the line path, due to the fact that the leader continuously changes its orientation, which requires the follower to continuously follow this changing behavior and track a point that is not “steady.” In this challenging scenario, the performance of the adaptive mechanism is always better than the performance of the nonadaptive strategy.

For better readability, the results in Tables II and III are summarized in histogram form in Fig. 4.

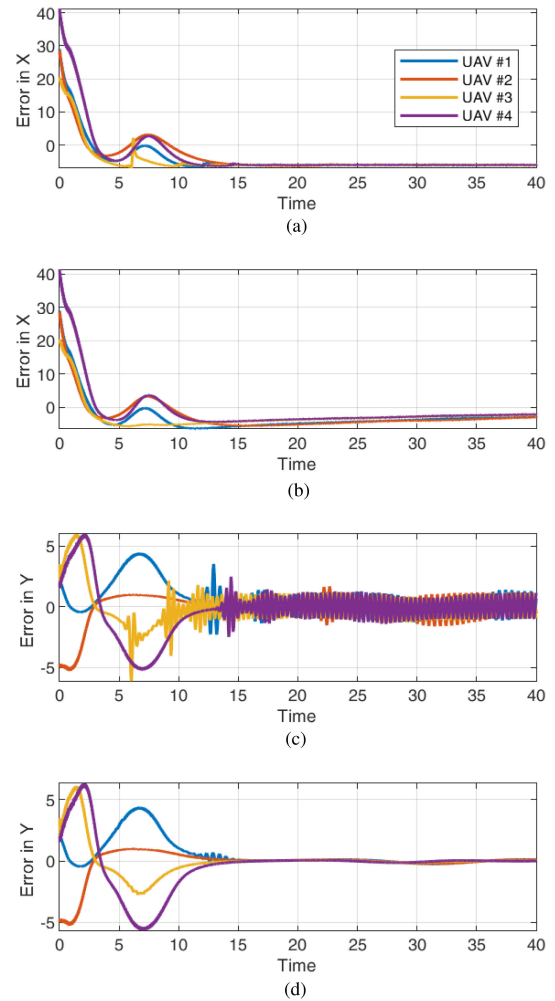


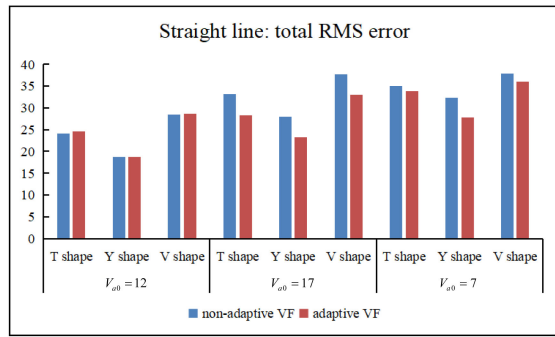
Fig. 7. Errors in straight line Y formation with $V_a = 12, V_{a0} = 17$. In the nonadaptive case the followers think the leader is faster than it actually is, and this leads to oscillations. (a) Nonadaptive VF: x error. (b) Adaptive VF: x error. (c) Nonadaptive VF: y error. (d) Adaptive VF: y error.

B. Discussion of Plots

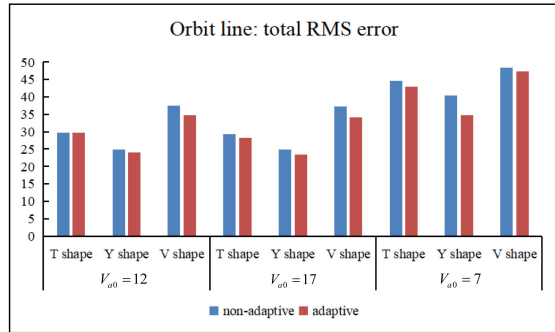
This section is meant to discuss some plots and clarify the reasons for such improvements. For a Y formation with $V_a = 12, V_{a0} = 17$ (the followers think that the leader is faster than it actually is), Figs. 5 and 6 show the performance for line path and orbit path, with and without adaptation. The total trajectories are shown, while the UAVs are “frozen” at the same time instant $t = 37$ s. The following conclusion can be drawn.

- 1) The nonadaptive strategy is not able to keep the Y shape: the leader is in red color in the middle of the Y shape and it can be seen that the follower right behind the leader is overlapping or almost colliding with the leader. This problem is avoided in the adaptive strategy.

For the same Y formation with $V_a = 12, V_{a0} = 17$ as above, Fig. 7 shows the evolution of the x, y errors. The following conclusions can be drawn.



(a)



(b)

Fig. 8. Each bar of the histogram show the sum rms errors for the four follower UAVs, using the distributed implementation of the proposed method (communication with neighbor according to the topology in Fig. 3). The sums are given for different neighbor speeds and shapes. The blue bar is the nonadaptive VF, the red bar is the adaptive VF. (a) Straight line path. (b) Orbit line path.

- 1) For the x error, it can be seen that a bias appears for the nonadaptive strategy, i.e., the error is not converging to zero. However, the adaptation mechanism of the adaptive strategy is able to drive such biases towards zero.
- 2) For the y error, it can be seen that oscillations appear for the nonadaptive strategy, i.e., the error oscillates around zero. However, the adaptation mechanism of the adaptive strategy suppresses such oscillations.

We conclude by showing that similar results as the ones reported before would be obtained also with the strategy in Section IV-D, i.e., with a distributed communication setting in which the leader-to-all communication is replaced by communication with a few neighboring UAVs (see the communication topologies in Fig. 3). To avoid repetitions, the details of these simulations are not given as in Tables II and III, but rather the results are summarized in the form of histograms in Fig. 8. Again, it can be seen that the adaptive strategy is comparable to the nonadaptive strategy when each UAV has correct knowledge of the neighbor velocity; then, the adaptive strategy outperforms the nonadaptive strategy when such knowledge becomes incorrect.

VI. CONCLUSION

A formation control protocol was studied in which the leader can communicate only its position and orientation. To compensate for the lack of knowledge of the leader velocity, a local estimator was designed for each UAV. Extensive simulations with different formation shapes have shown that the proposed adaptation mechanism has a very similar performance to the ideal case when the leader velocity is perfectly known, and outperforms all the nonadaptive cases in which the followers have incorrect knowledge of the leader velocity.

An interesting avenue for future work is to model the communication interference in UAVs (an open problem to the best of our knowledge) and study a mechanism to activate the estimator only when necessary. Another interesting problem is to perform real tests, which might induce studying new problems such as let the UAVs avoid collisions.

REFERENCES

- [1] T. S. No, Y. Kim, M.-J. Tahk, and G. E. Jeon, "Cascade-type guidance law design for multiple-UAV formation keeping," *Aerosp. Sci. Technol.*, vol. 15, no. 6, pp. 431–439, 2011.
- [2] F. Liao, R. Teo, J. L. Wang, and X. X. Dong, "Distributed formation and reconfiguration control of VTOL UAVs," *IEEE Trans. Control Syst. Technol.*, vol. 25, no. 1, pp. 270–277, Jan. 2017.
- [3] P. F. Lu, S. Baldi, G. R. Chen, and W. W. Yu, "Neuro-adaptive cooperative tracking rendezvous of nonholonomic mobile robots," *IEEE Trans. Circuits Syst. II: Exp. Briefs*, vol. 67, no. 12, pp. 3167–3171, Dec. 2020.
- [4] K. Harikumar, J. Senthilnath, and S. Sundaram, "Multi-UAV oxyrrhis Marina-inspired search and dynamic formation control for forest firefighting," *IEEE Trans. Autom. Sci. Eng.*, vol. 16, no. 2, pp. 863–873, Apr. 2019.
- [5] J. Yang, X. M. Wang, S. Baldi, S. Singh, and S. Fari, "A software-in-the-loop implementation of adaptive formation control for fixed-wing UAVs," *IEEE CAA J. Automatica Sinica*, vol. 6, no. 5, pp. 1230–1239, Sep. 2019.
- [6] Y. L. Liu, J. M. Montenbruck, D. Zelazo, and M. Odelga, "A Distributed control approach to formation balancing and maneuvering of multiple multirotor UAVs," *IEEE Trans. Robot.*, vol. 34, no. 4, pp. 870–882, Aug. 2018.
- [7] X. W. Fu, P. Jing, H. X. Wang, and X. G. Gao, "A formation maintenance and reconstruction method of UAV swarm based on distributed control," *Aerosp. Sci. Technol.*, vol. 104, Apr. 2020, Art. no. 105981.
- [8] A. Belkadi, H. Abaunza, L. Ciarletta, P. Castillo, and D. Theilliol, "Design and implementation of distributed path planning algorithm for a fleet of UAVs," *IEEE Trans. Aerosp. Electron. Syst.*, vol. 55, no. 6, pp. 2647–2657, Dec. 2019.
- [9] D. Brown and L. Sun, "Dynamic exhaustive mobile target search using unmanned aerial vehicles," *IEEE Trans. Aerosp. Electron. Syst.*, vol. 55, no. 6, pp. 3413–3423, Dec. 2019.

- [10] S. M. Khansari-Zadeh and F. Saghati
Vision-based navigation in autonomous close proximity operations using neural networks
IEEE Trans. Aerosp. Electron. Syst., vol. 47, no. 2, pp. 864–883, Apr. 2011.
- [11] U. Zengin and A. Dogan
Cooperative target pursuit by multiple UAVs in an adversarial environment
Robot. Auton. Syst., vol. 59, no. 12, pp. 1049–1059, 2011.
- [12] P. Panagiotou and K. Yakinthos
Aerodynamic efficiency and performance enhancement of fixed-wing UAVs
Aerosp. Sci. Technol., vol. 99, 2020, Art. no. 105575.
- [13] D. R. Nelson, D. B. Barber, T. W. McLain, and R. W. Beard
Vector field path following for miniature air vehicles
IEEE Trans. Robot., vol. 23, no. 3, pp. 519–529, Jun. 2007.
- [14] R. W. Beard, T. W. McLain, D. B. Nelson, D. Kingston, and D. Johanson
Decentralized Cooperative Aerial Surveillance Using Fixed-Wing Miniature UAVs
Proc. IEEE, vol. 94, no. 7, pp. 1306–1324, Jul. 2006.
- [15] A. Bosso, C. Conficoni, and A. Tilli
Multirotor UAV flight endurance and control: The drive perspective
In *Proc. IECON 2016-42nd Annu. Conf. IEEE Ind. Electron. Soc.*, 2016, pp. 1839–1845.
- [16] A. Bosso, C. Conficoni, D. Raggini, and A. Tilli
A computational-effective field-oriented control strategy for accurate and efficient electric propulsion of unmanned aerial vehicles
IEEE/ASME Trans. Mechatronics, vol. 26, no. 3, pp. 1501–1511, Jun. 2021.
- [17] N. Cho, S. Lee, J. Kim, Y. Kim, S. Park, and C. Song
Wind compensation framework for unpowered aircraft using online waypoint correction
IEEE Trans. Aerosp. Electron. Syst., vol. 56, no. 1, pp. 698–710, Feb. 2020.
- [18] L. Zhu, Y. Wang, and Z. Wu
An adaptive priority allocation for formation UAVs in complex context
IEEE Trans. Aerosp. Electron. Syst., vol. 57, no. 2, pp. 1002–1015, Apr. 2021.
- [19] C. Tabasso, N. Mimmo, V. Cichella, and L. Marconi
Optimal motion planning for localization of avalanche victims by multiple UAVs
IEEE Control Syst. Lett., vol. 5, no. 6, pp. 2054–2059, Dec. 2021.
- [20] A. Y. Mersha, S. Stramigioli, and R. Carloni
Exploiting the dynamics of a robotic manipulator for control of UAVs
In *Proc. IEEE Int. Conf. Robot. Autom.*, 2014, pp. 1741–1746.
- [21] B. Y. Zhou, H. Satyavada, and S. Baldi
Adaptive path following for unmanned aerial vehicles in time-varying unknown wind environments
In *Proc. Amer. Control Conf.*, 2017, pp. 1127–1132.
- [22] S. Fari, X. M. Wang, S. Roy, and S. Baldi
Addressing unmodelled path-following dynamics via adaptive vector field: A UAV test case
IEEE Trans. Aerosp. Electron. Syst., vol. 56, no. 2, pp. 1613–1622, Apr. 2019.
- [23] J. Wang, Z. Zhou, C. Wang, and Z. Ding
Cascade structure predictive observer design for consensus control with applications to UAVs formation flying
Automatica, vol. 121, 2020, Art. no. 109200.
- [24] H. Liu, Y. Lyu, and W. Zhao
Robust visual servoing formation tracking control for quadrotor UAV team
Aerosp. Sci. Technol., vol. 106, 2020, Art. no. 106061.
- [25] J. Seo, Y. Kim, S. Kim, and A. Tsourdos
Collision avoidance strategies for unmanned aerial vehicles in formation flight
IEEE Trans. Aerosp. Electron. Syst., vol. 53, no. 6, pp. 2718–2734, Dec. 2017.
- [26] X. W. Dong, B. H. Yu, Z. Y. Shi, and Y. S. Zhong
Time-varying formation control for unmanned aerial vehicles: theories and applications
IEEE Trans. Control Syst. Technol., vol. 23, no. 1, pp. 340–348, Jan. 2015.
- [27] X. W. Dong, Y. Z. Hua, Y. Zhou, Z. Ren, and Y. S. Zhong
Theory and experiment on formation-containment control of multiple multirotor unmanned aerial vehicle systems
IEEE Trans. Autom. Sci. Eng., vol. 16, no. 1, pp. 229–240, Jan. 2019.
- [28] O. Cetin and G. Yilmaz
Real-time autonomous UAV formation flight with collision and obstacle avoidance in unknown environment
J. Intell. Robot. Syst., vol. 84, pp. 415–433, 2016.
- [29] J. N. Wang and M. Xin
Integrated optimal formation control of multiple unmanned aerial vehicles
IEEE Trans. Control Syst. Technol., vol. 21, no. 5, pp. 1731–1744, Sep. 2013.
- [30] C. Zhao, X. Liu, S. Zhong, K. Shi, D. Liao, and Q. Zhong
Secure consensus of multi-agent systems with redundant signal and communication interference via distributed dynamic event-triggered control
ISA Trans., vol. 112, pp. 89–98, 2021, <https://doi.org/10.1016/j.isatra.2020.11.030>
- [31] Z. Li, T. Huang, Y. Tang, and W. Zhang
Formation control of multiagent systems with communication noise: A convex analysis approach
IEEE Trans. Cybern., vol. 51, no. 4, pp. 2253–2264, Apr. 2021.
- [32] H. Wang, H. Zhao, J. Zhang, D. Ma, J. Li, and J. Wei
Survey on unmanned aerial vehicle networks: A cyber physical system perspective
IEEE Commun. Surv. Tut., vol. 22, no. 2, pp. 1027–1070, Apr.–Jun. 2020.
- [33] W. Zheng, H. Wang, H. Ji, and J. Wu
UAV formation flight and collision warning with centralized control of ground control station
In *Proc. IEEE Int. Conf. Unmanned Syst.*, 2019, pp. 103–108.
- [34] T. Kim and K. Jerath
Congestion-aware cooperative adaptive cruise control for mitigation of self-organized traffic jams
IEEE Trans. Intell. Transp. Syst., to be published, doi: [10.1109/TITS.2021.3059237](https://doi.org/10.1109/TITS.2021.3059237).
- [35] A. Kliks *et al.*
Beyond 5 G: Big data processing for better spectrum utilization
IEEE Veh. Technol. Mag., vol. 15, no. 3, pp. 40–50, Sep. 2020.
- [36] J. Park, N. Cho, and S. Lee
Reactive collision avoidance algorithm for UAV using bounding tube against multiple moving obstacles
IEEE Access, vol. 8, pp. 218131–218144, 2020.
- [37] N. Cho and Y. Kim
Optimality of augmented ideal proportional navigation for maneuvering target interception
IEEE Trans. Aerosp. Electron. Syst., vol. 52, no. 2, pp. 948–954, Apr. 2016.
- [38] M. de Roo, P. Frasca, and R. Carloni
Optimal event handling by multiple unmanned aerial vehicles
In *Proc. IEEE Int. Conf. Robot. Autom.*, 2016, pp. 1230–1236.
- [39] M. R. Rosa
Leader-follower synchronization of uncertain Euler-Lagrange dynamics with Input constraints
Aerospace, vol. 7, no. 9, Art. no. 127, 2020.

- [40] A. Bosso, N. Mimmo, C. Conficoni, and A. Tilli
Global observability analysis of aided-INS for UAVs equipped with visual odometry systems
In *Proc. Eur. Control Conf.*, 2018, pp. 2909–2916.
- [41] S. Abdelmoeti and R. Carloni
Robust control of UAVs using the parameter space approach
In *Proc. IEEE/RSJ Int. Conf. Intell. Robots Syst.*, 2016, pp. 5632–5637.
- [42] Y. Hua, X. Dong, G. Hu, Q. Li, and Z. Ren
Distributed time-varying output formation tracking for heterogeneous linear multiagent systems with a nonautonomous leader of unknown input
IEEE Trans. Autom. Control, vol. 64, no. 10, pp. 4292–4299, Oct. 2019.
- [43] P. Zhou and B. M. Chen
Formation-containment control of Euler-Lagrange systems of leaders with bounded unknown inputs
IEEE Trans. Cybern., to be published.
- [44] X. Zhang, X. Yu, J. Lu, and W. Lan
Distributed leader-following formation control for mobile robots with unknown amplitudes of leader's velocity
In *Proc. 39th Chin. Control Conf.*, 2020, pp. 4889–4894.
- [45] P. Lu, H. Wang, F. Zhang, W. Yu, and G. Chen
Formation control of nonholonomic mobile robots using distributed estimators
IEEE Trans. Circuits Syst. II: Exp. Briefs, vol. 67, no. 12, pp. 3162–3166, Dec. 2020.
- [46] W. Lin
Distributed UAV formation control using differential game approach
Aerosp. Sci. Technol., vol. 35, no. 5, pp. 54–62, 2014.
- [47] D. Richert and J. Cortés
Optimal leader allocation in UAV formation pairs ensuring cooperation
Automatica, vol. 49, no. 11, pp. 3189–3198, 2012.
- [48] J. L. Zhang, J. G. Yan, and P. Zhang
Fixed-wing UAV formation control design with collision avoidance based on an improved artificial potential field
IEEE Access, vol. 6, pp. 78342–78351, 2018.
- [49] S. Baldi, S. Yuan, and P. Frasca
Output synchronization of unknown heterogeneous agents via distributed model reference adaptation
IEEE Control Netw. Syst., vol. 6, no. 2, pp. 515–525, Jun. 2019.
- [50] P. Ioannou and J. Sun
Robust Adaptive Control. New York, NY, USA: Dover, 2012.
- [51] P. Ioannou and K. Tsakalis
Linear Time-Varying Systems: Control and Adaptation, Englewood Cliffs, NJ, USA: Prentice Hall, 1992.
- [52] S. Fari
Guidance and control for a fixed-wing UAV
M.Sc. thesis, Scuola di Ingegneria Industriale e dell'Informazione, Politecnico Di Milano, Milan, Italy, 2017.



Simone Baldi (Senior Member, IEEE) received the B.Sc. degree in electrical engineering in 2005, the M.Sc. degree in automatic control engineering in 2005, and the Ph.D. degree in automatic control engineering in 2011, from the University of Florence, Florence, Italy.

He is a Professor with the School of Mathematics, Southeast University, Nanjing, China with guest position at Delft Center for Systems and Control (TU Delft). His research interests include adaptive and learning systems and intel-

ligent vehicles.

Dr. Baldi was awarded outstanding reviewer for *Automatica* in 2017. He is a Subject Editor of *International Journal of Adaptive Control and Signal Processing* (Wiley).



Danping Sun received the B.Sc. degree in information science from the Hubei University of Science and Technology, Hubei, China, in 2015, and she is currently working toward the postgraduate degree in electronic and electrical engineering with Wuhan Textile University, Wuhan, China.

Her research interests include adaptive systems and unmanned vehicles.



Guopeng Zhou received the B.Sc. degree in mathematics in 1994 from Hubei University, Wuhan, China, the M.Sc. and Ph.D. degrees in automation from the South China University of Technology, Guangzhou, China, in 2005 and 2008, respectively.

He is the Director of Hubei Electrical Machinery and Control System Engineering Technology Research Center, Xianning intelligent electromechanical industry alliance responsible person. His research interests include multiagent

systems, adaptive systems, intelligent mechanical and electrical systems, and fault diagnosis.



Di Liu received the B.Sc. degree in information science from the Hubei University of Science and Technology, Xianning, China, in 2014, and the M.Sc. degree in control science and engineering from the Chongqing University of Posts and Telecommunications, Chongqing, China, in 2017. She is currently working toward the double Ph.D. degrees, one in cyber science with the School of Cyber Science and Engineering, Southeast University, Nanjing, China, and one in systems and control with the Bernoulli Institute

for Mathematics, Computer Science and Artificial Intelligence, University of Groningen, Groningen, The Netherlands.

Her research interests include learning-based control for intelligent traffic, for automated vehicles, and unmanned vehicles.